2D/2D Heterostructure of Black Phosphorus/g-C_3N_4: Effective Ice-Assisted Synthesis and Metal-Free Photocatalyst for Efficient and Broadband H_2 Evolution

*Qingzhe Zhang, Shengyun Huang, Jiujun Deng, Zhenhe Xu, Giacomo Giorgi, Maurizia Palummo, Mohamed Chaker, and Dongling Ma**

Q. Zhang, S. Huang, Prof. Z. Xu, Prof. M. Chaker, Prof. D. Ma
Institut National de la Recherche Scientifique (INRS)-EMT
1650 Boulevard Lionel-Boulet, Varennes, Quebec J3X 1S2, Canada
E-mail: ma@emt.inrs.ca

Prof. J. Deng
Institute for Energy Research, Jiangsu University
Zhenjiang, Jiangsu 212013, P.R. China

Prof. Z. Xu
College of Applied Chemistry, Shenyang University of Chemical Technology
Shenyang, Liaoning 110142, P.R. China

Prof. G. Giorgi
Dipartimento di Ingegneria Civile e Ambientale (DICA), Università degli Studi di Perugia
Via G. Duranti, 06125 Perugia & CNR-ISTM, 06123 Perugia, Italy

Prof. M. Palummo
INFN, Department of Physics, Università degli Studi "Tor Vergata"
Via della Ricerca Scientifica 1, 00133 Roma, Italy

Keywords: ice-assisted exfoliation, metal-free photocatalysts, black phosphorous, g-C_3N_4, photocatalytic H_2 evolution

A two-dimensional (2D)/2D heterojunction of black phosphorous (BP)/graphitic carbon nitride (g-C_3N_4) photocatalyst (BP/g-C_3N_4) is designed and synthesized for water splitting. Ice-assisted exfoliation method developed herein for preparing BP nanosheets from bulk BP, which has not been previously reported yet, leads to high yield of few-layer BP nanosheets (~6 layers) with large lateral size, and greatly reduced duration and power for liquid exfoliation. The combination of BP with g-C_3N_4 not only protects BP from oxidation, but also contributes to largely enhanced photocatalytic activity both under $\lambda > 420$ nm and $\lambda > 475$ nm light irradiation, and long-term stability in water splitting for at least 120 h (the longest time period under current investigation). The H_2 production rate achieved by BP/g-C_3N_4 (384.17 μmol g^{-1} h^{-1}) is comparable to and even surpasses that of previously reported, precious metal loaded

photocatalyst under λ > 420 nm light. The efficient charge transfer between BP and g-C_3N_4 (highly likely due to the formation of N-P bonds) and broadening of photon absoprtion (as also supported by theoretical calculations) contribute to the high photocatalytic performance. The possible mechanism of H_2 evolution under different light irradiations is unveiled. This work presents a novel and facile method to prepare 2D nanomaterials, and provides a successful paradigm for the design of metal-free photocatalyst with improved charge-carrier dynamics for renewable energy conversion.

Solar water splitting for H_2 evolution has shown great potential as a green technology in solving energy crisis.[1] Taking economic and environmental factors into consideration, the development of efficient, low-cost, stable and nontoxic photocatalysts is highly desired and crucial for the widespread implementation of solar fuel technology. For acquiring the above listed beneficial features, visible-light-responsive graphitic carbon nitride (g-C_3N_4), a two-dimensional (2D) metal-free photocatalyst, has been extensively explored in photocatalysis. Though g-C_3N_4 was discovered to be feasible for photocatalytic water splitting, obtaining of the relatively high efficiency of H_2 evolution still largely relies on the loading of noble metal co-catalysts because of the high recombination rate of the charge carriers in g-C_3N_4.[2] Furthermore, the relatively wide bandgap (2.7 eV) confines its light response mainly into the ultraviolent (UV) range and only slightly into a small portion of the visible light range (λ < 460 nm).[3] To solve these problems, numerous strategies have been developed, mainly including morphology tuning, doping with metal/non-metal ions, and heterojunction creation.[4] However, quite limited progresses have been achieved thus far. Aiming to enhance the harvesting of solar light efficiently and economically, the development of novel g-C_3N_4-based metal-free photocatalysts with a broader photo-response range is of great significance.

Black phosphorus (BP), a layered material that consists of corrugated atomic planes with strong intra-layer chemical bonding and weak interlayer Van der Waals interactions, has attracted

tremendous interest of material scientists. Since the successful preparation of 2D BP with atom-thick layer in early 2014, it has provoked a surge of research with its enticing electrical and optical properties.[5] Differentiating from previously reported 2D nanomaterials, such as graphene, BP possesses tunable, thickness-dependent bandgaps that span from ~0.3 eV (bulk) to ~2.0 eV (monolayer) in addition to sufficiently high carrier mobility and photo-electronic response.[5b-d, 5f, 5g, 5i] These favorable properties render BP, particularly few-layer BP nanosheets (≤10 nm in thickness), a fascinating candidate for diverse applications in transistors, photodetectors, solar cells, bio-imaging and phototherapy.[5i, 6] Notably, BP has demonstrated its great potential as a broadband photocatalyst for the harvesting of solar energy due to its narrow and direct bandgap.[7] However, certain inherent problems existing in the typical, exfoliated BP nanosheets bring practical challenges for its actual application. For example, BP is very reactive to moisture and ambient oxygen, and can be easily oxidized due to the exposed lone pairs at its surface.[5f, 6e, 7e, 8] The roughening caused by the exfoliation can further accelerate surface oxidation, which may proceed exponentially during the first hour after exfoliation.[8b] As a consequence, the semiconducting properties of BP deteriorate rapidly, reflected from significantly increased contact resistance and reduced carrier mobility.[8a, 8b, 8e] It is thus of paramount importance to develop effective strategies to retard or, even better, eliminate the degradation of BP. Recently, several approaches were developed to protect BP from oxidation with various levels of success.[5i, 9] Among them, the non-covalent surface coverage of BP with other inert 2D materials, such as poly (methyl methacrylate), graphene or hexagonal boron nitride, was proposed as an effective way.[8e, 9b] Hence, it is rationally anticipated that the combination of BP with g-C_3N_4 nanosheets can highly likely yields both enhanced stability and broadband solar harvesting capability in photocatalytic water splitting for hydrogen evolution.

For the preparation of few-layer BP nanosheets, the mechanical and liquid exfoliation from bulk BP has been extensively used.[8a, 8c, 10] As BP possesses stronger interlayer interactions

compared with graphene and other 2D materials, the exfoliation by ultrasonication would be difficult and long processing time (>15 h) or a sonicator with high power are normally required.[8a, 8c, 10] Howbeit the yield of few-layer BP nanosheets is still very low.[8a, 10c] As the P-P bond is remarkably weaker than the C-C bond, such long duration or high power of sonication are known to generate nanosheets with reduced lateral size and anomalous structural defects.[8a, 11] In addition to the instability, such structural features can also accelerate charge carrier recombination and restrict the practical applications of BP in electronics and optoelectronics.

Herein, we present a novel, time-effective ice-assisted exfoliation method, for the first time, to prepare few-layer BP nanosheets. It led to the greatly improved yield of few-layer BP nanosheets, and largely reduced duration and power for liquid exfoliation from bulk BP. To gain long-term stability under ambient atmosphere, the few-layer BP and g-C_3N_4 nanosheets were integrated into a single, 2D-on-2D architecture (BP/g-C_3N_4). As a result, the oxidative degradation of BP was greatly inhibited. The as-synthesized metal-free BP/g-C_3N_4 photocatalysts exhibit high photocatalytic H_2 evolution efficiency from water and excellent stability under broadband light irradiation. This work opens a new path for the facile preparation of high-quality BP nanosheets with high yield and in short time and renders a great promise for BP-based photocatalysts for efficient solar water splitting.

To prepare BP nanosheets, bulk BP crystals are exfoliated in NMP using an NMP-ice-assisted ultrasonication method developed herein, which is detailed in the Experimental Section and schematically illustrated in **Figure 1**a. When the bulk BP powder is dispersed into NMP, the space between BP layers is filled with this solvent. As the melting point of NMP is -24 °C, after being placed into direct contact with liquid nitrogen bath, the dispersion starts to freeze. The gradually grown NMP ice crystals intercalate into BP layers to enlarge the interlayer spacing of BP, which largely reduces the interlayer Van der Waals interactions and is favourable for the next-step easy exfoliation to generate BP nanosheets. Subsequently, the frozen dispersion

undergoes ultrasonication, and the BP nanosheets are successfully exfoliated from the bulk BP. The ultrasonic vibration of NMP ice between the layers facilitates the exfoliation process. The required total time and the output power of the sonicator are less than 2 h and 70 W, respectively. Compared with the conventional liquid phase exfoliation,[8a, 8c, 10] both the processing time and sonication power are greatly reduced in our described method. As a result, the high-quality BP nanosheets with larger lateral size and less anomalous structural defects are obtained.[8a, 11] Furthermore, the high yield of the few-layer BP nanosheets was achieved with this unique approach. According to the ICP-AES analysis, 18.75 mg of few-layer BP nanosheets were obtained from 25 mg of bulk BP with the yield of 75%, which is much higher than the reported values (Table S1 in the Supporting Information). The obtained BP nanosheet-in-IPA dispersion is brown and very stable, and there is no aggregation and color change over four weeks during storage (Figure S1a-1b). To form the 2D-on-2D assembly, the g-C_3N_4 powder was introduced into the BP dispersion (Figure S1c). The large amount of precipitate was soon observed at the bottom of the solution with the supernatant turning to colorless and transparent after the incubation at room temperature for 30 min (Figure S1d), suggesting the successful integration and high coupling efficiency of BP with g-C_3N_4 nanosheets. Figure S1e presents the Zeta potentials of BP and g-C_3N_4 in IPA, which are positive and negative, respectively, at pH around 7 that is the pH value of coupling solution. It is clear that the strong electrostatic interaction between them contributes to their efficient integration.

The morphology of the as-prepared BP nanosheets was characterized by TEM. The typical TEM image of BP nanosheets shows a lamellar morphology with the lateral size of 50 nm-3 μm (Figure 1b and Figure S2a-d). Only the peaks of C, Cu and P elements were observed in the EDX spectrum (Figure 1c), indicating that the pure BP without any detectable oxidation was obtained *via* the NMP-ice-assisted exfoliation method. The thickness distribution of BP nanosheets was investigated using AFM height measurements (Figure 1d-f). Lines 1 and 2 in Figure 1d are randomly selected and their corresponding height profiles are displayed in Figure

1e. Assuming the thickness of a monolayer BP is 0.53 nm,[6a, 6b, 8d] the number of layers of the generated BP nanosheets could be estimated from the AFM height measurements. Figure 1f shows the statistical histogram of the number of BP layers, which was obtained from the height profiles of 150 randomly selected individual BP nanosheets in AFM images. The mean number of layers was determined to be <*N*> = 5.9±1.5, and about 93% of the observed BP nanosheets have the thickness of less than 10 nm. The large pieces observed in AFM images are due to single thicker BP or stacking of several BP sheets during sample preparation.

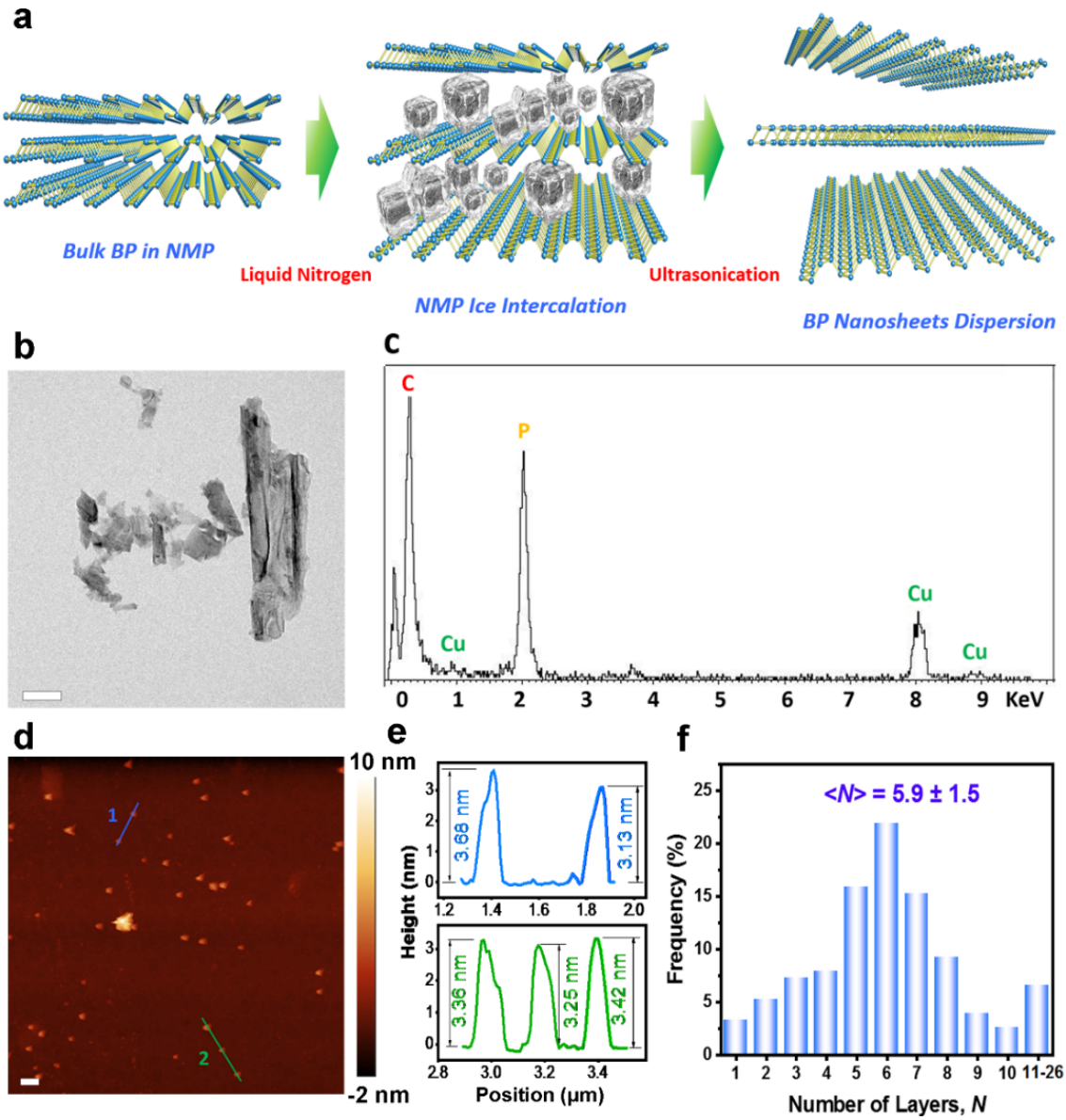

Figure 1. a) Schematic illustration of the preparation of BP nanosheets with NMP-ice-assisted exfoliation method. b) TEM image of BP nanosheets and c) EDX spectrum of b). d) Tapping mode AFM topographical image of few-layer BP nanosheets. Scale bars in b) and d) are 500 nm. e) Height profiles of BP nanosheets along the blue Line 1 and green Line 2 in d). f)

Distribution of BP layers calculated from the height profiles of 150 BP nanosheets in AFM images.

The g-C_3N_4 shows a free-standing graphene-like wrinkled nanosheet structure (**Figure 2**a). As displayed in Figure 2b-2d, the initial morphologies of BP and g-C_3N_4 nanosheets were remained after their integration. The nanosheets marked with arrows in Figure 2d are supposed to be BP considering their relatively "regular" edges, which is further corroborated by the high-angle annular dark field (HAADF) scanning TEM (STEM) image (Figure 2e) and corresponding STEM-EDX elemental mappings (Figure 2f-2i). The STEM-EDX mapping of C, N and P clearly confirms the co-existence of g-C_3N_4 and BP, and shows the stacking and the close interaction of these two components. The high-resolution TEM (HRTEM) image reveals lattice fringes of 0.34 nm and 0.26 nm, attributed to the (021) and (040) planes of the BP crystals (Figure 2j).[6e] The presence of C, N and P peaks indicates the successful preparation of BP/g-C_3N_4 hybrid nanosheets with high purity and without detectable oxidative degradation (Figure 2g), which is consistent with the STEM-EDX mapping results and is further verified by the following XPS analysis.

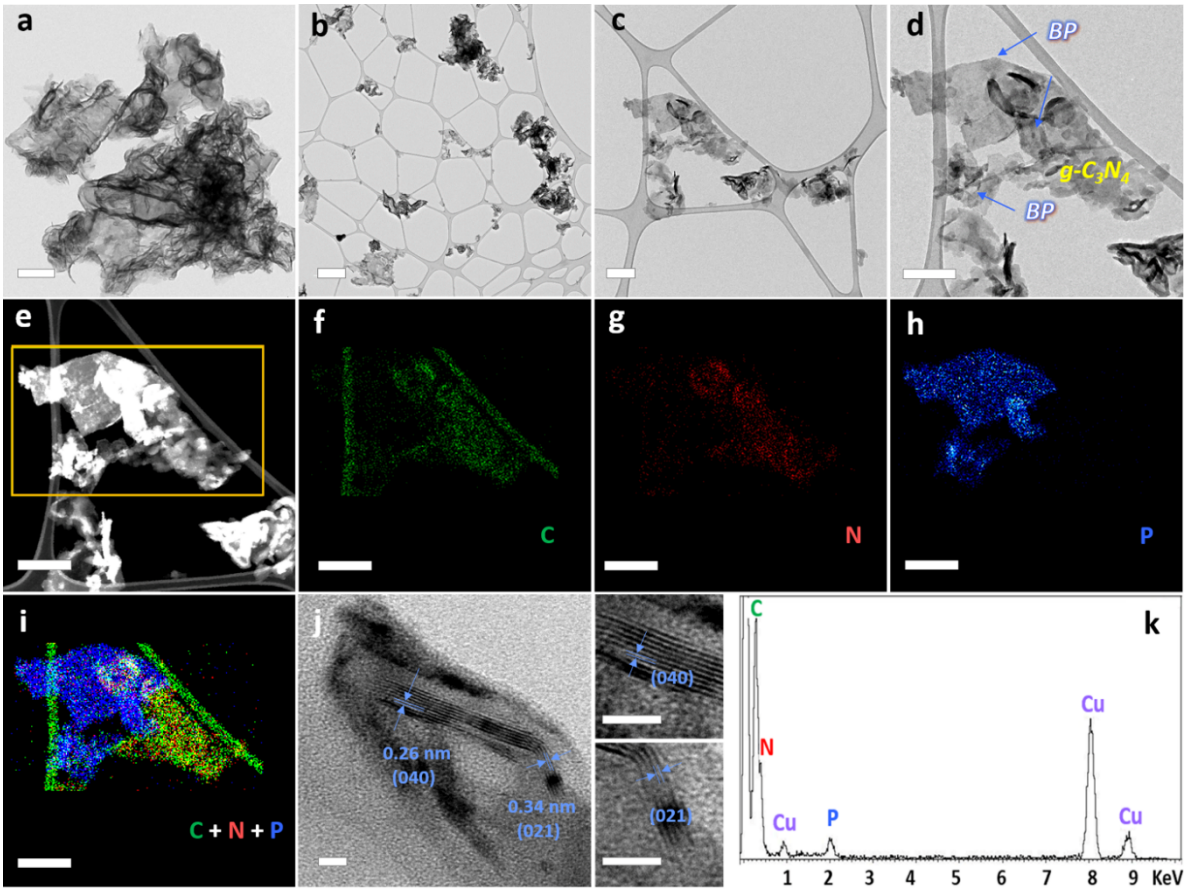

Figure 2. Representative TEM images of (a) g-C_3N_4 and (b-d) BP/g-C_3N_4 with different magnifications. (e) High-angle annular dark field (HAADF) scanning TEM (STEM) image of (d), (f-i) STEM-EDX mapping of C, N, P, and the overlay of all the elements of the selected area in (e). (j) HRTEM image of BP/g-C_3N_4, and (k) EDX spectrum of (j). Scale bars: (a) and (c-i), 250 nm; (b), 1 μm; (j), 5 nm. The TEM grids used in (a), (j) and (k) are carbon film coated copper grids, and those used in the other figures are lacey carbon film coated nickel grids.

The composition and the chemical states of the as-prepared samples were assessed using XPS (**Figure 3** and Figure S3). In the XPS survey spectra of BP/g-C_3N_4 (Figure S3), only the peaks assigned to C, N, O and P elements were observed, signifying the high purity of the prepared samples and the successful integration of BP and g-C_3N_4 nanosheets. As previously reported, O1s peak was observed in the XPS spectrum of g-C_3N_4, which is attributed to the O element in the adsorbed O_2 or H_2O on the sample surface.[14] The similar atomic O percentages of g-C_3N_4 (3.61%) and BP/g-C_3N_4 (3.59%) strongly support that no further oxidation occurred in the preparation of BP/g-C_3N_4 hybrid sample (Table S2). In addition, the concentration of P in BP/g-C_3N_4 nanosheets was detected to be 3.3% by XPS, which is quite close to that of 3.2% measured by ICP-AES and the nominal value of 3.0%. All these results suggest the remarkable coupling

efficiency between BP and g-C_3N_4 nanosheets. To specify the bond formation in the prepared BP/g-C_3N_4 sample, peak deconvolution was performed for the C1s, N1s and P2p XPS spectra (Figure 3a-3c). The high-resolution C1s XPS spectrum presents two distinct peaks at 284.8 and 288.3 eV (Figure 3a), which can be assigned to the graphitic sp^2 C=C bonds in the surface adventitious carbon contaminations and in the C-N aromatic heterocycles, respectively.[4c, 15] The main N1s peak was deconvoluted into three peaks (Figure 3b), located at 398.6, 399.4 and 401.1 eV, which are assigned to the sp^2 hybridized N in triazine rings (C=N-C), tertiary N (N-$(C)_3$) and amino group (C-N-H), respectively.[16] As shown in Figure 3c, the fitting result of P2p spectrum shows two peaks at binding energies of 129.8 and 130.6 eV, corresponding to $P2p_{3/2}$ and $P2p_{1/2}$, respectively. Compared with the two peaks in the P2p XPS spectrum of BP, the shifts toward lower binding energies were observed in that of BP/g-C_3N_4, indicating an increase of the electron density of P atoms, highly likely due to partial electron transfer from N atoms. Similar observation has been reported by others and it supports the strong interfacial interaction between BP and g-C_3N_4, which is supposed to introduce shallow charge trapping sites and suppress charge carrier recombination and thus beneficial for photocatalysis.[7c, 17] This is quite different from deep trapping sites, which can facilitate charge recombination and are detrimental to photocatalysis,[18] It is noteworthy that the peak in the range of 133.5~134.0 eV, ascribed to oxidized P (P_xO_y),[7c, 7d, 19] was not observed in the P2p XPS spectra of either BP or BP/g-C_3N_4, indicating that P was not considerably oxidized during both the exfoliation process of bulk BP to BP nanosheets and the preparation process of BP/g-C_3N_4 hybrid sample. The developed, time-efficient NMP-ice-assisted exfoliation method played a vital role in protecting BP from oxidation by largely shortening the ultrsonication time and further reducing the possibility of exposure to O_2.

Figure 3d shows the XRD patterns of bulk BP, exfoliated BP nanosheets, g-C_3N_4 and BP/g-C_3N_4 samples. The diffraction peaks shown in the patterns of bulk BP and BP nanosheets can be well indexed to the orthorhombic BP with space group Cmca (64) according to the standard

pattern of BP (JCPDS No. 73-1358).[6d, 6f] Furthermore, the lower-angle peak originated from the periodic stacking of layers exhibits a downshift from 16.95° of the BP bulk counterpart to 15.89° of the exfoliated BP nanosheets, corresponding to the inter-plane distance increasing from 5.2 Å to 5.6 Å, respectively (inset of Figure 3d). This result verifies that the intercalation of NMP ice crystals can enlarge the inter-planar spacing of BP, and further benefit its easy exfoliation by reducing the interlayer Van der Waals interactions. In the XRD pattern of g-C_3N_4, the two peaks present at 13.0° and 27.4° are ascribed to the in-planar arrangement of the tri-s-triazine unit and the inter-planar stacking of the conjugated aromatic system, respectively.[2a, 3b, 4c, 16c, 20] For the diffractogram of BP/g-C_3N_4 sample, both the characteristic diffraction peaks of BP and g-C_3N_4 were observed, explicitly confirming their successful integration once again. No additional diffraction peaks were observed, implying no new crystalline phases or compounds are formed during the coupling reaction.

The optical properties of BP nanosheets in IPA, g-C_3N_4 and BP/g-C_3N_4 nanosheets were investigated as displayed in the UV-vis-NIR absorption spectra (Figure 3e). The BP nanosheets show a quite broad absorption band from UV to NIR regions, whilst g-C_3N_4 exhibits a typical semiconductor-like absorption spectrum in the UV and blue regions with the absorption edge of around 466 nm. Through the Tauc plots (Figure S4), the bandgap energy (E_g) of as-prepared BP and g-C_3N_4 nanosheets were estimated to be ~1.39 eV and ~2.66 eV, respectively.

Figure 3f shows the theoretical Tauc-plot curves obtained from the ab-initio absorbance spectra calculated for BP of different layer thickness (1-4 and 6 layers). They were calculated by performing state-of-the-art Many-Body Perturbation theory calculations (namely GW method and Bethe-Salpeter equation) [12] on top of density functional theory (DFT) simulations.[13] The geometries of the layered structures have been obtained using norm conserving pseudopotentials[21] and Perdew-Burke-Ernzerhof (PBE) exchange-correlation functional with Van der Waals correction,[22] able to reproduce with very good accuracy the structural lattice parameters of bulk BP. The vacuum in the aperiodic direction has been selected to be larger

than 15 Å for monolayer and bilayer and for all the other cases larger than the thickness of the few-layer phosphorene atomic structure. Although a direct comparison with the experimental curve shown in Figure S4a is quite difficult, due to the presence at experimental level of several thicknesses and to the assumption, at theoretical level of perfect isolated layers in a vacuum dielectric screening, the broad feature from visible to NIR is in line with what experimentally observed and supports the experimental estimation of an average thickness of about 6 layers. It is worth to underline that the calculated optical gaps can be better extracted from the position of the first optical peak in the absorption curves (Figure S5) and are due to bound excitons. The binding energies decrease with the increasing number of BP layers, due to the smaller quantum confinement effect and larger dielectric screening. Indeed the calculated GW electronic (transport) gaps (Figure S6) are systematically larger than the energetic position of the first optical peaks.[8a, 23]

For the BP/g-C_3N_4 2D-on-2D assembled nanosheet photocatalyst, in addition to the absorption of g-C_3N_4, a largely enhanced tail absorption in the visible and NIR regions was clearly observed due to the introduction of BP nanosheets. This can greatly benefit the visible light-driven photocatalytic water splitting for H_2 production. Furthermore, a slight red-shift of the absorption edge was observed in the spectrum of BP/g-C_3N_4 (474 nm) compared to that of g-C_3N_4 (466 nm), confirming the strong N-P interactions between BP and g-C_3N_4.

The photocatalytic H_2 production from water splitting in the presence of BP, g-C_3N_4, 3% BP/g-C_3N_4 and 10% BP/g-C_3N_4 photocatalysts under $\lambda > 420$ nm light irradiation and the stability measurement of BP/g-C_3N_4 are shown in Figure 3g-3h. All the samples show H_2 evolution from water containing triethanolamine, which acts as the sacrificial electron donor to quench the photoinduced holes. The as-prepared BP/g-C_3N_4 photocatalyst exhibits much larger H_2 evolution amount (93.14 μmol), compared to that of BP (13.18 μmol) and g-C_3N_4 samples (20.43 μmol) after 24 h of light irradiation. As displayed in Figure 3h, the highest H_2 evolution rate was achieved by BP/g-C_3N_4 (384.17 μmol g^{-1} h^{-1}), which is about 7 times and 4.5 times

higher than that of pure BP (54.88 μmol g^{-1} h^{-1}) and g-C_3N_4 (86.23 μmol g^{-1} h^{-1}). The fast recombination of photo-generated charge carriers in BP and g-C_3N_4 should be responsible for their poor photocatalytic activities. In the BP/g-C_3N_4 composite, the excited electrons in the conduction band (CB) of g-C_3N_4 are possibly transferred to BP nanosheets and suppress the recombination of charge carriers in g-C_3N_4, and further enhance the photocatalytic activity, which were confirmed by the following constructed energy diagrams. Under $\lambda > 420$ nm light irradiation, the excitation of g-C_3N_4 plays the major role in water splitting. When BP content increases to 10%, the g-C_3N_4 content is accordingly reduced, leading to a decreased H_2 evolution rate (271.2 μmol g^{-1} h^{-1}). The H_2 production rate achieved by 3% BP/g-C_3N_4 is comparable to or even higher than that of the reported photocatalyst with the loading of the precious metal Pt as a co-catalyst (Table S3). Furthermore, only about 2% decrease was observed in the H_2 evolution by the as-synthesized BP/g-C_3N_4 photocatalyst after 120 h (the longest time period under the current investigation) of visible light irradiation, suggesting that it possesses excellent stability in water under light illumination. The P2p XPS spectra of BP and BP/g-C_3N_4 after photocatalytic experiment were measured (Figure S7). An additional peak at ~134 eV, assigned to the oxidized P, appeared after water splitting, which accounts for 21.6 at% and 7.5 at% of P in BP and BP/g-C_3N_4, respectively (Table S4), indicating that the introduction of g-C_3N_4 greatly inhibits the oxidation of BP by ~3 times. Though a small portion of P in BP/g-C_3N_4 was oxidized, the photocatalytic activity was not distinctively affected.

Figure 3i shows the photocatalytic H_2 production by the prepared samples under $\lambda > 475$ nm light irradiation. No H_2 was detected in the presence of bare BP, g-C_3N_4 or 3% BP/g-C_3N_4 photocatalysts, while 10% BP/g-C_3N_4 sample exhibits H_2 generation rate of 143.47 μmol g^{-1} h^{-1} (Figure S8). When BP loading content increases to 15%, no obvious further enhancement was observed in H_2 evolution. In this scenario ($\lambda > 475$ nm irradiation), g-C_3N_4 cannot be excited and only BP excitation contributes to water splitting, but the fast charge carrier recombination in BP greatly decreases its photocatalytic activity. As a result, both g-C_3N_4-only and BP-only

samples show inferior activity. The combination of BP and g-C_3N_4 may introduce shallow interfacial charge trap sites, which can promote the charge separation in BP.[18] It well explains the clearly observed photoactivity with BP loading of 10% and 15% with respect to plain g-C_3N_4 and BP samples. However, higher loading (15% *vs* 10%) does not necessarily lead to higher activity due to the limited trap sites. These results suggest that the as-prepared BP/g-C_3N_4 is an economic, efficient and stable, completely metal-free photocatalyst, without introducing any metal as co-catalyst, for H_2 evolution from water splitting under broadband light irradiation.

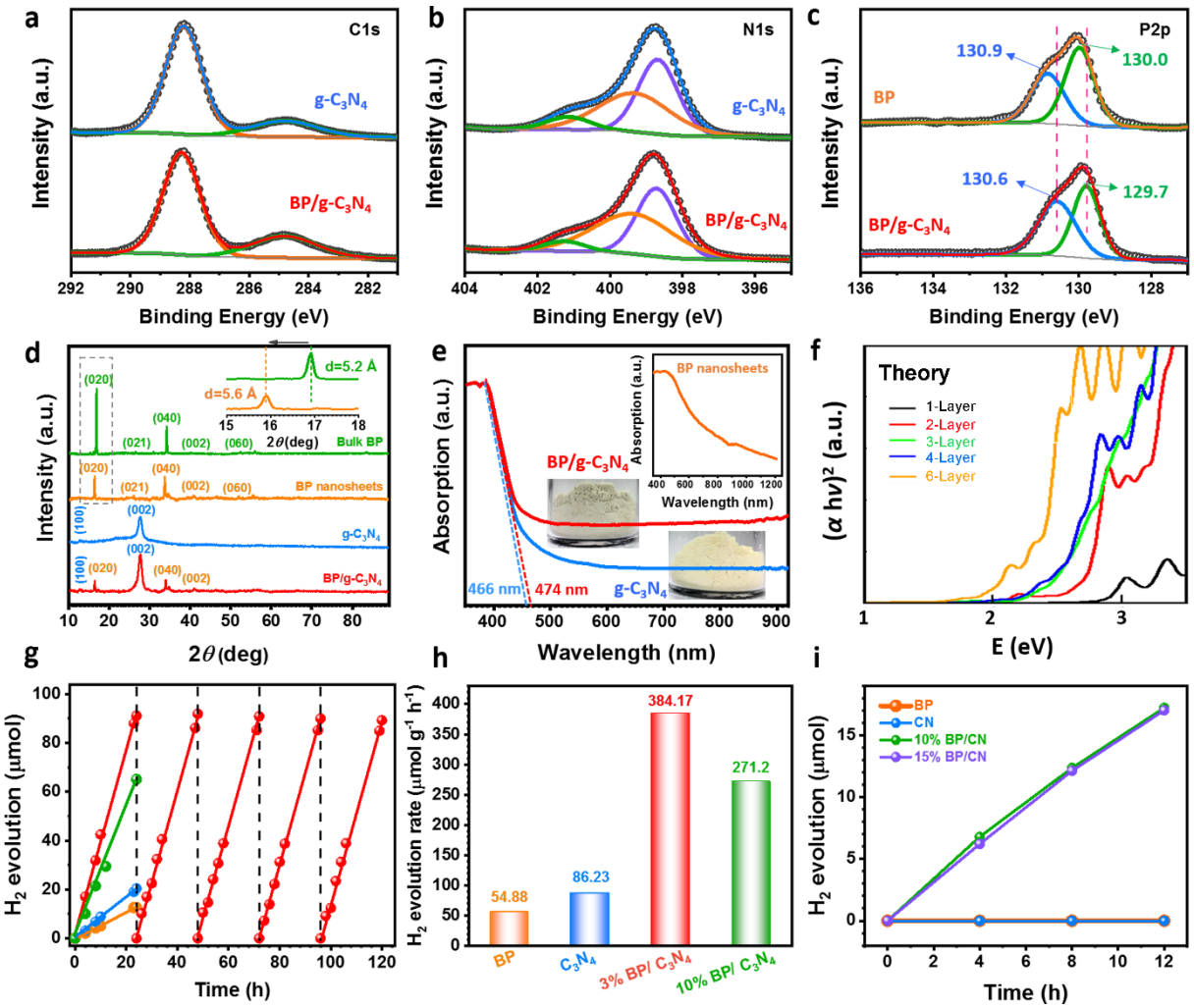

Figure 3. High-resolution (a) C1s and (b) N1s XPS spectra of g-C_3N_4 and BP/g-C_3N_4, and (c) P2p XPS spectra of BP and BP/g-C_3N_4 samples. (d) XRD patterns of bulk BP, BP nanosheets, g-C_3N_4 and BP/g-C_3N_4 samples. The inset is the amplification of XRD patterns of bulk BP and BP nanosheets in the lower-angle range, which is marked by the dashed rectangle in (d). (e) UV-vis-NIR absorption spectra of g-C_3N_4 and BP/g-C_3N_4 powder samples. Insets in (e) are the absorption spectrum of BP nanosheets in dispersion (top), photos of BP/g-C_3N_4 (middle) and

g-C_3N_4 (bottom) powders. (f) Theoretical Tauc-plot curves of BP with different layer numbers (1-4 and 6 layers). (g, i) Photocatalytic water splitting for H_2 evolution and (h) H_2 evolution rate achieved in the presence of BP (orange), g-C_3N_4 (blue), 3% BP/g-C_3N_4 (red),10% BP/g-C_3N_4 (green) and 15% BP/g-C_3N_4 (purple) photocatalysts under (g-h) $\lambda > 420$ nm and (i) $\lambda > 475$ nm light irradiations.

The PEC properties of the as-prepared g-C_3N_4 and BP/g-C_3N_4 samples were evaluated by electrochemical impedance spectroscopy (EIS) and transient photocurrent responses (**Figure 4**a-4b). Some useful information for the charge transfer resistance can be extracted from the high frequency region of Nyquist plots. The significantly decreased arc radii are exhibited in the EIS Nyquist plots of BP/g-C_3N_4 compared with that of g-C_3N_4 both in the dark and under simulated solar light irradiation (Figure 4a), suggesting that the introduction of BP leads to the increase of the interfacial charge transfer rate in the BP/g-C_3N_4 sample.[2d, 3b, 16c, 24] To further verify the improved PEC performance, the transient photocurrent responses for more than ten light on-off cycles were measured under simulated solar light irradiation (Figure 4b). The photocurrent density rapidly increases to a saturation value and remains constant once the light is switched on, and immediately returns to nearly zero when the light is turned off. The saturated photocurrent density of BP/g-C_3N_4 ($\sim$5.28 μA cm^{-2}) is about 4.8 times higher than that of plain g-C_3N_4 photocatalysts ($\sim$1.11 μA cm^{-2}). The increased photocurrent density strongly verifies that the introduction of BP nanosheets can facilitate charge separation/transport,[2d, 25] and/or enhance the visible light absorption due to their narrower bandgap. Altogether they contribute to the improved photocatalytic H_2 evolution rate of water splitting under visible light irradiation. It is worth noting that almost no decrease in the photocurrent density was observed after about 2000 s of the light on-off tests, which supports that the as-synthesized g-C_3N_4 and BP/g-C_3N_4 samples possess good stability under light irradiation.

To better understand the nature of BP/g-C_3N_4 as an efficient photocatalyst for H_2 evolution, UPS measurements were performed to determine the energy levels of BP and g-C_3N_4 nanosheets (Figure 4c-4d). The intersections of the extrapolated linear portion at high and low binding energies with the baseline give the edges of the UPS spectra, from which the UPS

widths of BP and g-C_3N_4 are determined to be 15.99 eV and 14.95 eV, respectively.[15a] Then the VB energy (E_{VB}) values of BP and g-C_3N_4 are estimated to be 5.23 eV and 5.96 eV, respectively, by subtracting the width of the UPS spectra from the excitation energy (21.22 eV). Combining with the measured E_g from the absorption spectra, the CB energy values (E_{CB}) of BP (4.18 eV) and g-C_3N_4 (3.3 eV) are estimated from $E_{CB}= E_{VB}-E_g$.[7c, 15a] These values in eV are all converted to electrochemical energy potentials in V according to the reference standard for which –4.44 eV *vs.* vacuum level equals 0 V *vs.* reversible hydrogen electrode (RHE).[15a]

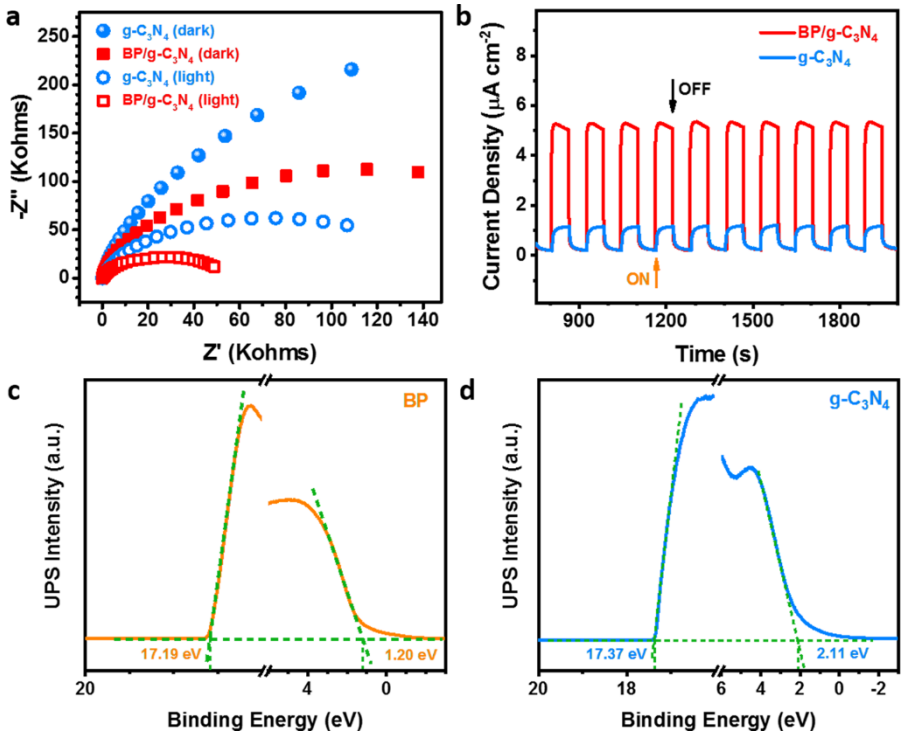

Figure 4. (a) EIS Nyquist plots of g-C_3N_4 and BP/g-C_3N_4 with and without illumination. (b) Transient photocurrent density response of g-C_3N_4 and BP/g-C_3N_4 during light on/off cycles under a 0.2 V bias versus Ag/AgCl electrode. Valence band UPS cut-off spectra of (c) BP and (d) g-C_3N_4 samples.

Based on the UPS measurement results, the possible mechanism for the largely enhanced photocatalytic activity in H_2 evolution of BP/g-C_3N_4 photocatalysts is proposed. As schematically illustrated in **Scheme 1**, the CB energy level of BP is more positive (-0.60 V) than that of g-C_3N_4 (-1.18 V), and both of them are more negative than the reduction potential of H^+/H_2 (~0 V). In addition, the VB energy level of BP is higher than that of g-C_3N_4. These properly positioned bands are suitable for the transfer of charge carriers for water splitting,

corroborating the capability of BP/g-C_3N_4 as a metal-free photocatalyst for H_2 evolution. Under λ>420 nm light irradiation, mainly the electrons in the VB of g-C_3N_4 are excited to its CB, leaving behind the positive-charged holes in the VB (Scheme 1a). Afterwards, the excited electrons can be further transferred into the CB of adjacent BP, largely suppressing the recombination of charge carriers and promoting the reduction of H_2O to produce H_2. In addition to benefiting from the suitable energy levels of BP and g-C_3N_4, the charge transfer process is also efficiently promoted by the presence of certain trap sites. At the same time, the holes in the VB of g-C_3N_4 can be immediately captured by the hole-sacrificial agent TEOA to generate its oxide. In this process, BP mainly plays a role as the electron acceptor to inhibit the charge carrier recombination and leads to efficient H_2 evolution. In this case, BP absorption and the presence of interfacial trap states also contribute to the enhanced photocatalytic activity, but are not dominating owing to their much smaller ratio than g-C_3N_4. Under λ>475 nm light irradiation, the excitation of g-C_3N_4 can be excluded. BP cannot by itself act as the effective photocatalyst either, for water splitting due to its fast charge carrier recombination. While in the BP/g-C_3N_4 composite, the excited electrons in the CB of BP are captured by the interfacial trap sites and participate in the H_2 evolution from water splitting (Scheme 1b). Simultaneously, the holes left behind in the VB of BP are scavenged by TEOA to generate CO_2 and water.

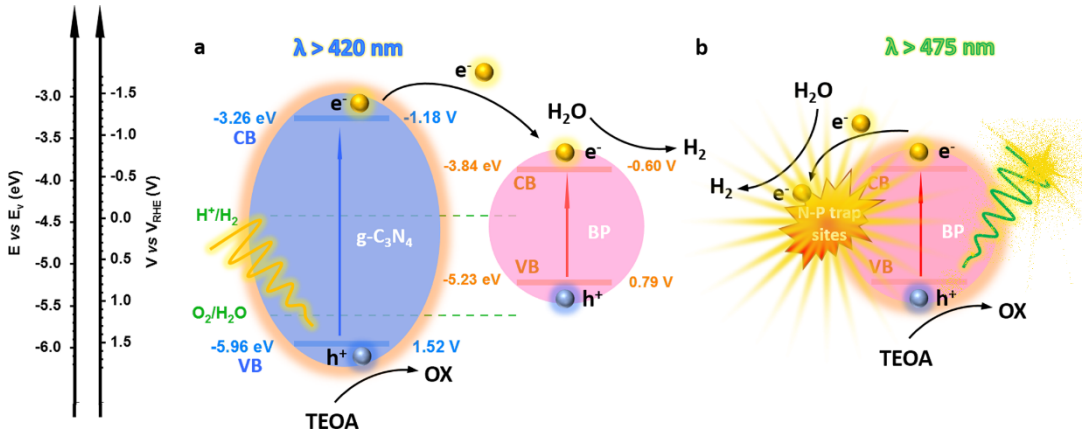

Scheme 1. Schematic energy diagram of BP/g-C_3N_4 photocatalyst and proposed possible mechanism for the photocatalytic H_2 evolution from water splitting under (a) λ > 420 nm and (b) λ > 475 nm light irradiation.

In conclusion, a novel metal-free efficient BP/g-C_3N_4 visible light photocatalyst was developed. The NMP-ice-assisted exfoliation method was presented for the first time to prepare few-layer BP nanosheets from bulk BP, which leads to high yield of few-layer BP nanosheets with large lateral size and largely reduced duration and power for liquid exfoliation. The combination of BP with g-C_3N_4 leads to largely enhanced photocatalytic activity in H_2 evolution from water splitting under both $\lambda > 420$ nm and $\lambda > 475$ nm light irradiation. The intensive interaction at the interface of BP and g-C_3N_4 greatly promotes charge transfer from excited g-C_3N_4 to BP, which can also introduce the interfacial trap sites to capture the electrons from excited BP for water splitting. Furthermore, the introduction of g-C_3N_4 protects BP from oxidation and the as-prepared BP/g-C_3N_4 photocatalyst shows excellent long-term stability in photocatalytic water splitting. This work provides a facile preparation approach of high-quality BP nanosheets and renders a successful paradigm for the design of metal-free photocatalyst with improved charge-carriers dynamics for efficient and broadband water splitting.

Supporting Information
Supporting Information is available from the Wiley Online Library or from the author.

Acknowledgements
Financial support from the Natural Sciences and Engineering Research Council of Canada (NSERC) in the context of NSERC-Discovery Grant and NSERC-Strategic Grant (with the support of Canadian Solar Inc.), and le Fonds de recherche du Quebec-Nature et technologies (FRQNT) is greatly appreciated. M.C. is also grateful to the Canada Research Chairs Program. In addition, Q.Z. acknowledges the support under State Scholarship Fund from the China Scholarship Council (CSC, No. 201506220152), Z.X. acknowledges the National Natural Science Foundation of China (NSFC 51402198) and Natural Science Foundation of Liaoning Province (201602592) for financial support. M.P. thanks INFN for financial support through the National project Nemesys and for allocated computational resources at CINECA. G. G. acknowledges PRACE (Grant No. Pra17_4466 "DECONVOLVES") and ISCRA ("2D-OIHPs" HP10BGUJ6X and "ExMoxC" HP10CMVPR7) for awarding access to resource Marconi based in Italy at CINECA.

Conflict of Interest
The authors declare no conflict of interest.

Received: ((will be filled in by the editorial staff))
Revised: ((will be filled in by the editorial staff))
Published online: ((will be filled in by the editorial staff))

References

[1] a) A. Fujishima, K. Honda, *Nature* **1972**, *238*, 37; b) K. Maeda, K. Teramura, D. L. Lu, T. Takata, N. Saito, Y. Inoue, K. Domen, *Nature* **2006**, *440*, 295; c) A. Kudo, Y. Miseki, *Chem. Soc. Rev.* **2009**, *38*, 253; d) Q. Zhang, D. Thrithamarassery Gangadharan, Y. Liu, Z. Xu, M. Chaker, D. Ma, *J. Materiomics* **2017**, *3*, 33.

[2] a) X. Wang, K. Maeda, A. Thomas, K. Takanabe, G. Xin, J. M. Carlsson, K. Domen, M. Antonietti, *Nat. Mater.* **2009**, *8*, 76; b) G. G. Zhang, Z. A. Lan, X. C. Wang, *Angew. Chem., Int. Ed.* **2016**, *55*, 15712; c) H. H. Ou, P. J. Yang, L. H. Lin, M. Anpo, X. C. Wang, *Angew. Chem., Int. Ed.* **2017**, *56*, 10905; d) D. Zheng, X. N. Cao, X. Wang, *Angew. Chem., Int. Ed.* **2016**, *55*, 11512; e) Z. Xu, M. G. Kibria, B. AlOtaibi, P. N. Duchesne, L. V. Besteiro, Y. Gao, Q. Zhang, Z. Mi, P. Zhang, A. O. Govorov, L. Mai, M. Chaker, D. Ma, *Appl. Catal., B* **2018**, *221*, 77.

[3] a) J. S. Zhang, X. F. Chen, K. Takanabe, K. Maeda, K. Domen, J. D. Epping, X. Z. Fu, M. Antonietti, X. C. Wang, *Angew. Chem., Int. Ed.* **2010**, *49*, 441; b) Q. Zhang, J. Deng, Z. Xu, M. Chaker, D. Ma, *ACS Catal.* **2017**, *7*, 6225.

[4] a) X. F. Chen, J. S. Zhang, X. Z. Fu, M. Antonietti, X. C. Wang, *J. Am. Chem. Soc.* **2009**, *131*, 11658; b) L. Sun, M. J. Yang, J. F. Huang, D. S. Yu, W. Hong, X. D. Chen, *Adv. Funct. Mater.* **2016**, *26*, 4943; c) V. W.-h. Lau, I. Moudrakovski, T. Botari, S. Weinberger, M. B. Mesch, V. Duppel, J. Senker, V. Blum, B. V. Lotsch, *Nat. Commun.* **2016**, *7*, 12165; d) W. J. Ong, L. L. Tan, Y. H. Ng, S. T. Yong, S. P. Chai, *Chem. Rev.* **2016**, *116*, 7159; e) J. Fu, J. Yu, C. Jiang, B. Cheng, *Adv. Energy Mater.* **2018**, *8*, 1701503.

[5] a) Y. X. Deng, Z. Luo, N. J. Conrad, H. Liu, Y. J. Gong, S. Najmaei, P. M. Ajayan, J. Lou, X. F. Xu, P. D. Ye, *ACS Nano* **2014**, *8*, 8292; b) L. Li, Y. Yu, G. J. Ye, Q. Ge, X. Ou, H. Wu, D. Feng, X. H. Chen, Y. Zhang, *Nat. Nanotechnol.* **2014**, *9*, 372; c) H. Liu, A. T. Neal, Z. Zhu, Z. Luo, X. F. Xu, D. Tomanek, P. D. Ye, *ACS Nano* **2014**, *8*, 4033; d) E. S. Reich, *Nature* **2014**, *506*, 19; e) F. N. Xia, H. Wang, D. Xiao, M. Dubey, A. Ramasubramaniam, *Nat. Photonics* **2014**, *8*, 899; f) X. Ling, H. Wang, S. X. Huang, F. N. Xia, M. S. Dresselhaus, *PNAS*

2015, *112*, 4523; g) L. Z. Kou, C. F. Chen, S. C. Smith, *J. Phys. Chem. Lett.* **2015**, *6*, 2794; h) H. Liu, Y. C. Du, Y. X. Deng, P. D. Ye, *Chem. Soc. Rev.* **2015**, *44*, 2732; i) C. R. Ryder, J. D. Wood, S. A. Wells, Y. Yang, D. Jariwala, T. J. Marks, G. C. Schatz, M. C. Hersam, *Nat. Chem.* **2016**, *8*, 598.

[6] a) F. N. Xia, H. Wang, Y. C. Jia, *Nat. Commun.* **2014**, *5*, 4458; b) M. Buscema, D. J. Groenendijk, S. I. Blanter, G. A. Steele, H. S. J. van der Zant, A. Castellanos-Gomez, *Nano Lett.* **2014**, *14*, 3347; c) J. Sun, G. Y. Zheng, H. W. Lee, N. Liu, H. T. Wang, H. B. Yao, W. S. Yang, Y. Cui, *Nano Lett.* **2014**, *14*, 4573; d) H. Wang, X. Z. Yang, W. Shao, S. C. Chen, J. F. Xie, X. D. Zhang, J. Wang, Y. Xie, *J. Am. Chem. Soc.* **2015**, *137*, 11376; e) Z. Sun, H. Xie, S. Tang, X. F. Yu, Z. Guo, J. Shao, H. Zhang, H. Huang, H. Wang, P. K. Chu, *Angew. Chem., Int. Ed.* **2015**, *54*, 11526; f) X. Zhang, H. Xie, Z. Liu, C. Tan, Z. Luo, H. Li, J. Lin, L. Sun, W. Chen, Z. Xu, L. Xie, W. Huang, H. Zhang, *Angew. Chem., Int. Ed.* **2015**, *54*, 3653; g) Y. Yang, J. Gao, Z. Zhang, S. Xiao, H. H. Xie, Z. B. Sun, J. H. Wang, C. H. Zhou, Y. W. Wang, X. Y. Guo, P. K. Chu, X. F. Yu, *Adv. Mater.* **2016**, *28*, 8937.

[7] a) M. Z. Rahman, C. W. Kwong, K. Davey, S. Z. Qiao, *Energy Environ. Sci.* **2016**, *9*, 709; b) W. Y. Lei, T. T. Zhang, P. Liu, J. A. Rodriguez, G. Liu, M. H. Liu, *ACS Catal.* **2016**, *6*, 8009; c) M. Zhu, S. Kim, L. Mao, M. Fujitsuka, J. Zhang, X. Wang, T. Majima, *J. Am. Chem. Soc.* **2017**, *139*, 13234; d) M. S. Zhu, X. Y. Cai, M. Fujitsuka, J. Y. Zhang, T. Majima, *Angew. Chem., Int. Ed.* **2017**, *56*, 2064; e) X. J. Zhu, T. M. Zhang, Z. J. Sun, H. L. Chen, J. Guan, X. Chen, H. X. Ji, P. W. Du, S. F. Yang, *Adv. Mater.* **2017**, *29*, 1605776; f) W. Hu, L. Lin, R. Zhang, C. Yang, J. Yang, *J. Am. Chem. Soc.* **2017**, *139*, 15429.

[8] a) A. H. Woomer, T. W. Farnsworth, J. Hu, R. A. Wells, C. L. Donley, S. C. Warren, *ACS Nano* **2015**, *9*, 8869; b) A. Ziletti, A. Carvalho, D. K. Campbell, D. F. Coker, A. H. C. Neto, *Phys. Rev. Lett.* **2015**, *114*, 046801; c) J. Kang, J. D. Wood, S. A. Wells, J. H. Lee, X. L. Liu, K. S. Chen, M. C. Hersam, *ACS Nano* **2015**, *9*, 3596; d) A. Favron, E. Gaufres, F. Fossard, A. L. Phaneuf-L'Heureux, N. Y. W. Tang, P. L. Levesque, A. Loiseau, R. Leonelli, S. Francoeur,

R. Martel, *Nat. Mater.* **2015**, *14*, 826; e) A. Hirsch, F. Hauke, *Angew. Chem., Int. Ed.* **2017**, *57*, 4338.

[9] a) J. D. Wood, S. A. Wells, D. Jariwala, K. S. Chen, E. Cho, V. K. Sangwan, X. L. Liu, L. J. Lauhon, T. J. Marks, M. C. Hersam, *Nano Lett.* **2014**, *14*, 6964; b) R. A. Doganov, E. C. T. O'Farrell, S. P. Koenig, Y. T. Yeo, A. Ziletti, A. Carvalho, D. K. Campbell, D. F. Coker, K. Watanabe, T. Taniguchi, A. H. C. Neto, B. Ozyilmaz, *Nat. Commun.* **2015**, *6*, 6647; c) W. N. Zhu, M. N. Yogeesh, S. X. Yang, S. H. Aldave, J. S. Kim, S. Sonde, L. Tao, N. S. Lu, D. Akinwande, *Nano Lett.* **2015**, *15*, 1883; d) Y. T. Zhao, H. Y. Wang, H. Huang, Q. L. Xiao, Y. H. Xu, Z. N. Guo, H. H. Xie, J. D. Shao, Z. B. Sun, W. J. Han, X. F. Yu, P. H. Li, P. K. Chu, *Angew. Chem., Int. Ed.* **2016**, *55*, 5003.

[10] a) J. R. Brent, N. Savjani, E. A. Lewis, S. J. Haigh, D. J. Lewis, P. O'Brien, *Chem. Commun.* **2014**, *50*, 13338; b) P. Yasaei, B. Kumar, T. Foroozan, C. H. Wang, M. Asadi, D. Tuschel, J. E. Indacochea, R. F. Klie, A. Salehi-Khojin, *Adv. Mater.* **2015**, *27*, 1887; c) L. Chen, G. M. Zhou, Z. B. Liu, X. M. Ma, J. Chen, Z. Y. Zhang, X. L. Ma, F. Li, H. M. Cheng, W. C. Ren, *Adv. Mater.* **2016**, *28*, 510.

[11] M. Batmunkh, C. J. Shearer, M. J. Biggs, J. G. Shapter, *J. Mater. Chem. A* **2016**, *4*, 2605.

[12] P. Giannozzi, S. Baroni, N. Bonini, M. Calandra, R. Car, C. Cavazzoni, D. Ceresoli, G. L. Chiarotti, M. Cococcioni, I. Dabo, A. Dal Corso, S. de Gironcoli, S. Fabris, G. Fratesi, R. Gebauer, U. Gerstmann, C. Gougoussis, A. Kokalj, M. Lazzeri, L. Martin-Samos, N. Marzari, F. Mauri, R. Mazzarello, S. Paolini, A. Pasquarello, L. Paulatto, C. Sbraccia, S. Scandolo, G. Sclauzero, A. P. Seitsonen, A. Smogunov, P. Umari, R. M. Wentzcovitch, *J. Phys.-Condens. Matter* **2009**, *21*, 395502.

[13] A. Marini, C. Hogan, M. Gruning, D. Varsano, *Comput. Phys. Commun.* **2009**, *180*, 1392.

[14] a) F. Dong, Z. W. Zhao, T. Xiong, Z. L. Ni, W. D. Zhang, Y. J. Sun, W. K. Ho, *ACS Appl. Mater. Interfaces* **2013**, *5*, 11392; b) Y. Q. Cao, Z. Z. Zhang, J. L. Long, J. Liang, H. Lin, H. X. Lin, X. X. Wang, *J. Mater. Chem. A* **2014**, *2*, 17797.

[15] a) J. Liu, Y. Liu, N. Y. Liu, Y. Z. Han, X. Zhang, H. Huang, Y. Lifshitz, S. T. Lee, J. Zhong, Z. H. Kang, *Science* **2015**, *347*, 970; b) H. J. Kong, D. H. Won, J. Kim, S. I. Woo, *Chem. Mater.* **2016**, *28*, 1318.

[16] a) C. Ye, J.-X. Li, Z.-J. Li, X.-B. Li, X.-B. Fan, L.-P. Zhang, B. Chen, C.-H. Tung, L.-Z. Wu, *ACS Catal.* **2015**, *5*, 6973; b) J. Q. Zhang, X. H. An, N. Lin, W. T. Wu, L. Z. Wang, Z. T. Li, R. Q. Wang, Y. Wang, J. X. Liu, M. B. Wu, *Carbon* **2016**, *100*, 450; c) G. Peng, L. Xing, J. Barrio, M. Volokh, M. Shalom, *Angew. Chem., Int. Ed.* **2017**, *56*, 1; d) H. J. Yu, R. Shi, Y. X. Zhao, T. Bian, Y. F. Zhao, C. Zhou, G. I. N. Waterhouse, L. Z. Wu, C. H. Tung, T. R. Zhang, *Adv. Mater.* **2017**, *29*, 1605148.

[17] X. G. Li, W. T. Bi, L. Zhang, S. Tao, W. S. Chu, Q. Zhang, Y. Luo, C. Z. Wu, Y. Xie, *Adv. Mater.* **2016**, *28*, 2427.

[18] T. Leijtens, G. E. Eperon, S. Pathak, A. Abate, M. M. Lee, H. J. Snaith, *Nat. Commun.* **2013**, *4*, 2885.

[19] M. Zhu, Z. Sun, M. Fujitsuka, T. Majima, *Angew. Chem., Int. Ed.* **2018**, *57*, 1.

[20] a) D. J. Martin, P. J. T. Reardon, S. J. A. Moniz, J. W. Tang, *J. Am. Chem. Soc.* **2014**, *136*, 12568; b) Q. Han, B. Wang, J. Gao, Z. Cheng, Y. Zhao, Z. Zhang, L. Qu, *ACS Nano* **2016**, *10*, 2745.

[21] M. Schlipf, F. Gygi, *Comput. Phys. Commun.* **2015**, *196*, 36.

[22] S. Grimme, *J. Comput. Chem.* **2006**, *27*, 1787.

[23] a) Y. Zeng, X. Liu, C. Liu, L. Wang, Y. Xia, S. Zhang, S. Luo, Y. Pei, *Appl. Catal., B* **2018**, *224*, 1; b) D. Y. Qiu, F. H. da Jornada, S. G. Louie, *Nano Lett.* **2017**, 17, 4706.

[24] M. X. Li, W. J. Luo, D. P. Cao, X. Zhao, Z. S. Li, T. Yu, Z. G. Zou, *Angew. Chem., Int. Ed.* **2013**, *52*, 11016.

[25] D. Shi, R. Zheng, M. J. Sun, X. Cao, C. X. Sun, C. J. Cui, C. S. Liu, J. Zhao, M. Du, *Angew. Chem., Int. Ed.* **2017**, *56*, 14637.

A green and facile strategy was developed to generate few-layer black phosphorus (BP): ice-assisted exfoliation from bulk BP. A metal-free photocatalyst was synthesized by combining BP and g-C_3N_4, which protected BP from oxidation and led to efficient and broadband activity as well as long-term stability in H_2 evolution. Benefiting from formed N-P bonds, the efficient charge transfer between them yields excellent photocatalytic performance.

Keyword: ice-assisted exfoliation, metal-free photocatalysts, black phosphorous, g-C_3N_4, photocatalytic H_2 evolution

Q. Zhang, S. Huang, J. Deng, Z. Xu, G. Giorgi, M. Palummo, M. Chaker, D. Ma*

2D/2D Heterostructure of Ice-Assisted Synthesized Black Phosphorus/g-C_3N_4: A Metal-Free Photocatalyst for Efficient and Broadband H_2 Evolution

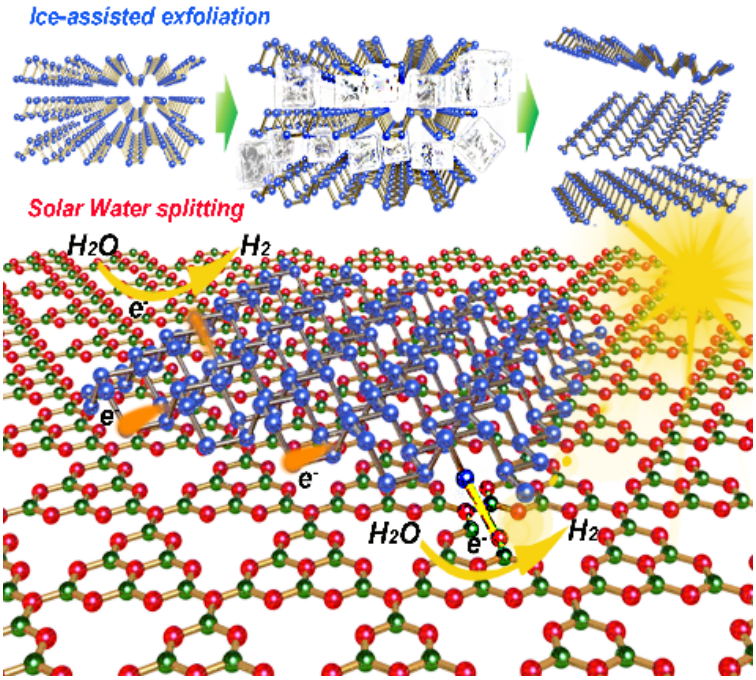

ToC figure (55 mm broad × 50 mm high)

Supporting Information

2D/2D Heterostructure of Ice-Assisted Synthesized Black Phosphorus/g-C_3N_4: A Metal-Free Photocatalyst for Efficient and Broadband H_2 Evolution

*Qingzhe Zhang, Shengyun Huang, Jiujun Deng, Zhenhe Xu, Giacomo Giorgi, Maurizia Palummo, Mohamed Chaker, and Dongling Ma**

Q. Zhang, S. Huang, Prof. Z. Xu, Prof. M. Chaker, Prof. D. Ma
Institut National de la Recherche Scientifique (INRS)-EMT
1650 Boulevard Lionel-Boulet, Varennes, Quebec J3X 1S2, Canada
E-mail: ma@emt.inrs.ca

Prof. J. Deng
Institute for Energy Research, Jiangsu University
Zhenjiang, Jiangsu 212013, P.R. China

Prof. G. Giorgi
Dipartimento di Ingegneria Civile e Ambientale (DICA), Università degli Studi di Perugia
Via G. Duranti, 06125 Perugia & CNR-ISTM, 06123 Perugia, Italy

Prof. M. Palummo
INFN, Department of Physics, Università degli Studi "Tor Vergata"
via della Ricerca Scientifica 1, 00133 Roma, Italy

Experimental Section

Materials. BP crystals of high-purity (~99.998%) were purchased from Smart Elements, N-Methyl-2-pyrrolidone (NMP, 99.5%, anhydrous), isopropanol (IPA, 99.5%, anhydrous), urea (NH_2CONH_2), nitric acid (HNO_3), N,N-Dimethylformamide (DMF) and triethanolamine (≥99.0%) were purchased from Sigma-Aldrich and used as received without further purification. The ultrapure water (18.2 MΩ cm, 25 °C), obtained from a Millipore Ultrapure water system, was used throughout the current study.

NMP-Ice-Assisted Preparation of BP Nanosheets. BP nanosheets were synthesized by developing a NMP-ice-assisted exfoliation method. Specifically, 25 mg of bulk BP was ground into fine powder and dispersed into 25 mL of NMP solvent. The dispersion was completely

frozen with a liquid nitrogen bath for 5-10 min, and then sonicated in a bath sonicator (BRANSONIC, 70 W, 40 kHz) for ~10 min to make the "NMP ice" melt. The procedure of freezing and melting was repeated 3 times. To protect the BP from oxygen and water, the dispersion was sealed in a vial, and all the experimental manipulations were performed in a glovebox or with nitrogen bubbling. Afterwards, the dispersion was centrifuged at 7000 rpm for 15 min to remove the residual un-exfoliated BP. The light yellow supernatant was decanted gently, which was the dispersion of BP nanosheets in NMP. The obtained BP nanosheets were washed with IPA by centrifugation at 12000 rpm for 2 times. The collected precipitate was re-dispersed into 25 mL of IPA. The concentration of BP in this dispersion was determined to be 0.75 mg mL^{-1} by Inductively Coupled Plasma Atomic Emission Spectroscopy (ICP-AES).

Preparation of g-C_3N_4 Nanosheets. The g-C_3N_4 nanosheets were synthesized by our reported thermal polymerization method.[1] Generally, urea (30 g) was placed into a covered alumina crucible and then heated in a quartz tube furnace with a heating rate of 2 °C min^{-1} to 250, 350, and 550 °C, and maintained at these three target temperatures for 1, 2, and 2 h, respectively. After being naturally cooled down to room temperature, the yellow powder was collected and washed for three times with HNO_3 (0.1 mol L^{-1}) and water to remove potential alkaline residue (e.g., ammonia). After centrifugation, the precipitate was dried in the vacuum at 80 °C overnight.

Preparation of BP/g-C_3N_4 Photocatalysts. BP/g-C_3N_4 nanosheets were prepared by dispersing 10 mg of g-C_3N_4 powder into 0.4 mL of BP nanosheet dispersion in IPA. The mixture was stirred for 2 h to couple BP nanosheets with g-C_3N_4 nanosheets under the protection of N_2. Subsequently, the sample was collected by centrifugation at 6000 rpm for 5 min, and then washed completely with IPA. The final product was obtained by drying the washed sample in an oven under vacuum at 60 °C overnight. The obtained BP/g-C_3N_4 nanosheets contain 3 % BP, and the composites with different weight percentages were prepared with adding different volumes of BP dispersion.

Characterization. A transmission electron microscope (TEM, JEOL 2100F), equipped with an energy-dispersive X-ray (EDX) spectrometer, was employed and operated at an accelerating voltage of 200 kV to study the microstructure and composition of the prepared samples. The topography image of the BP nanosheets on the pre-cleaned glass was observed by an atomic force microscopy (AFM, Bruker, MultiMode 8) in a tapping mode. Zeta potential of the as-prepared BP and g-C_3N_4 nanosheets in IPA was recorded with a Brookhaven ZetaPlus system in a standard 10 mm all-side-transparent polymethyl methacrylate cuvette. The crystalline structure was analyzed by an X-ray diffraction system (XRD, PANalytical X'Pert MRD, operated at 45 kV and 40 mA) with a Cu Kα radiation source (λ = 0.15406 nm). X-ray photoelectron spectroscopy (XPS) was taken on a VG Escalab 220i-XL spectrometer equipped with a twin anode Al Kα radiation X-ray source. All the XPS spectra were calibrated with the C1s peak at 284.8 eV as reference. Ultraviolet photoelectron spectroscopy (UPS) measurements were carried out with an unfiltered Helium (21.22 eV) gas discharge lamp to determine the valence band (VB) position of as-prepared BP and g-C_3N_4 samples. The UV-visible-near infrared (UV-vis-NIR) absorption spectra of g-C_3N_4, BP nanosheets and BP/g-C_3N_4 powder were obtained using a scan spectrometer (Varian Cary 5000) equipped with an integrating sphere. The bandgap energy (E_g) of the prepared g-C_3N_4 and BP nanosheets were determined from the Tauc plots, *i.e.* $(\alpha h\nu)^2$ as a function of $h\nu$. The concentration of BP nanosheets in IPA dispersion and the content of BP in the composites were determined by an IRIS Intrepid II XSP ICP-AES (Thermal Scientific, USA).

Photoelectrochemical Measurements. Photoelectrochemical (PEC) properties were measured with a standard three electrode system in an electrochemical workstation (CHI 660E, CH Instruments). The working electrode was prepared by coating the as-synthesized sample on fluorine-doped tin oxide (FTO) glass with its boundaries being protected by Scotch tape. Specifically, 2 mg of powder sample was dispersed into 2 mL of DMF under sonication for 30 min to obtain evenly dispersed slurry, which was drop-casted onto the FTO glass. After drying

under ambient condition, the epoxy resin glue was used to isolate the uncoated part of the FTO glass. A Pt wire and a Ag/AgCl electrode were used as the counter and reference electrode, respectively. The 0.2 M of Na_2SO_4 (pH = 6.8) aqueous solution pre-purged with nitrogen for 30 min was used as an electrolyte. A solar simulator equipped with an AM1.5G filter (LCS-100, Newport) was utilized as the light source. Nyquist plots were recorded over the frequency range of 100 mHz to 100 kHz at a bias of 0.2 V.

Photocatalytic H_2 Evolution. Photocatalytic H_2 evolution experiment was performed in a 500 mL Pyrex top-irradiation reactor with a quartz cover. A 300 W Xenon lamp equipped with cut-off filters (420 nm and 475 nm) was used to provide the irradiation source in the visible wavelength range. Typically, 10 mg of photocatalysts were dispersed in 100 mL of aqueous solution containing 10% of triethanolamine (TEOA) as sacrificial reagents. The mixture was deaerated by N_2 gas for 20 min and sonicated for 5 min. The system was sealed and vacuumed prior to photocatalysis. During the irradiation, the suspension was stirred continuously and kept at a constant temperature by circulating cooling water. The evolved H_2 was analyzed by a gas chromatography (GC, 7890B, Agilent Technologies) equipped with a thermal conductivity detector. For stability measurements, the photocatalysts were collected from the final reaction slurry by centrifugation, and then washed with ethanol and water thoroughly. Subsequently, the recycled sample underwent the photocatalytic H_2 evolution experiment under the identical conditions and repeated for 5 cycles with a total irradiation time of 120 h.

Theoretical Calculations. Calculated absorption spectra (Fig. 3f) were obtained by performing Many-Body Perturbation theory calculations (namely GW method and Bethe-Salpeter equation) [2] on top of density functional theory (DFT) simulations.[3] In the G_oW_o simulations we used a cutoff of 40 Ry to expand the wavefunctions, 160 Ry to evaluate the difference between the exchange self-energy and exchange-correlation matrixelements $<\sum_x - V_{xc}>$. For the screening term W and the correlation self-energy matrixelements $<\sum_c>$ we performed careful convergence tests for the monolayer finding that 12 Ry and 400 bands provide well

converged gaps within 0.05 eV. We further checked that using lower convergence parameters, namely 6 Ry and 100 bands in G the gap correction reduces of about 0.1 eV. For the same system we verified that performing partial self-consistency in the Green Function as GW_0 scheme the gap increases of about 0.1 eV. In order to speed up the calculations we performed, for all the other systems, calculations using a cutoff of 6 Ry and N_b= (N)*100 (N number of layers) bands and avoiding self-consistency. We then added the estimated difference of 0.2 eV, after verifying that this value really occurs for the case of the bilayer. The convergence on k-points has been carefully checked both at GW and BSE level and a grid of 24×21×1 is enough to converge both quantities within 0.1 eV. A box-like cutoff in the coulomb potential, as implemented in the yambo code, has been used to avoid spurious interactions between the images and speed up the convergence with the vacuum size.

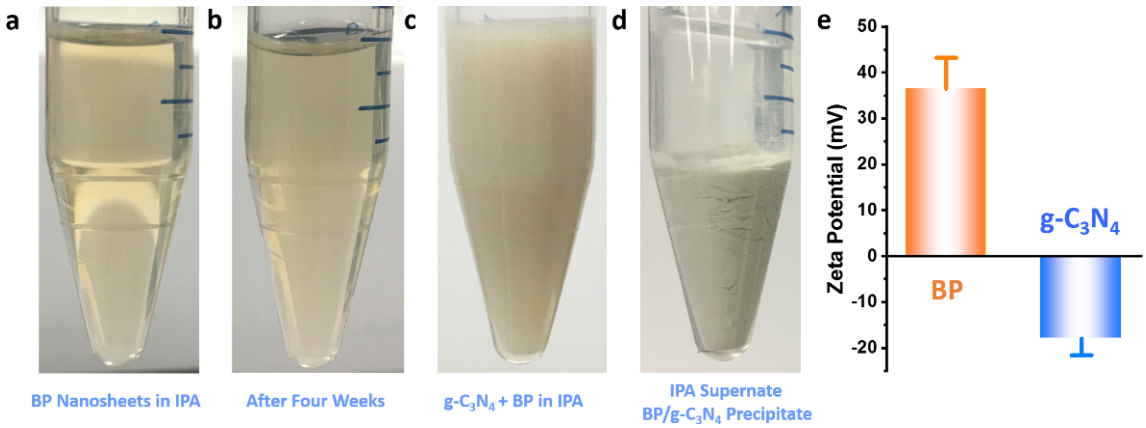

Figure S1. Photographs of BP nanosheets in isopropanol (IPA) a) at the first day, b) after four weeks, c) after adding g-C_3N_4, and d) after the incubation at room temperature for 30 min. e) The zeta potentials of BP and g-C_3N_4 nanosheets in IPA at pH around 7.

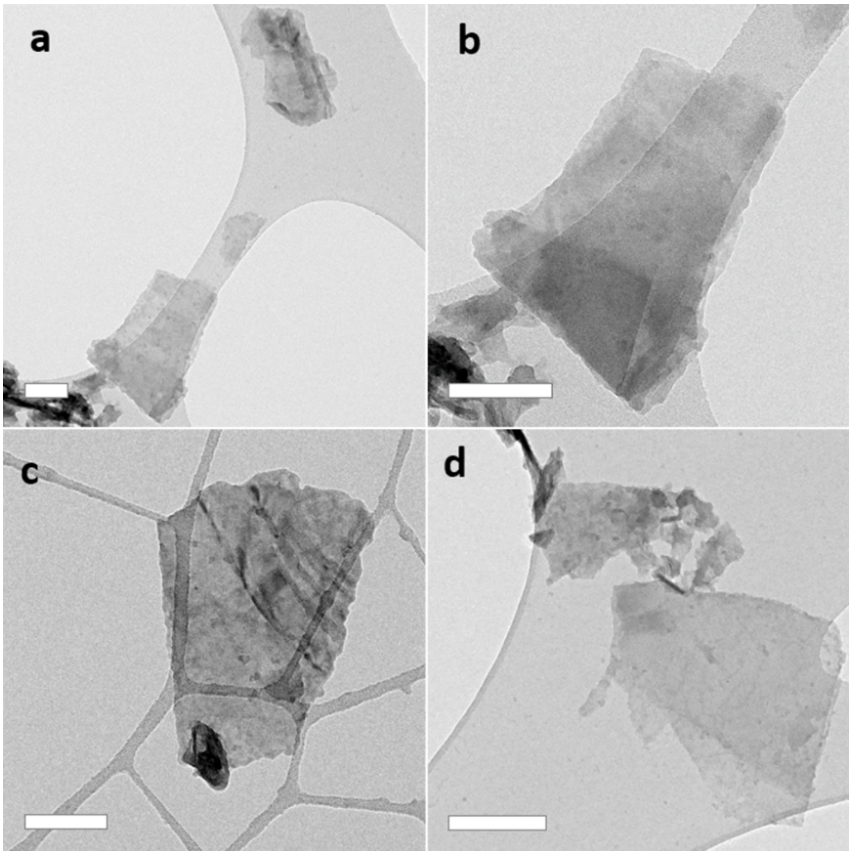

Figure S2. TEM images of BP nanosheets with different magnifications (Scale bar: 500 nm).

Table S1. Comparison of the yield of few-layer BP nanosheets from different exfoliation methods.

Reference	Sonication Bath		Tip Sonicator		Few-layer BP yield
	Power/W	Time/h	Power/W	Time/h	
ACS Nano, 2015, 9, 8869 [4]	70	13			26%
Adv. Mater. 2016, 28, 510 [5]	380	20			30%
ACS Catal. 2016, 6, 8009 [6]	-	8			15%
J. Am. Chem. Soc. 2017, 139, 13234 [7]			10	4	20%
Angew. Chem. Int. Ed. 2018, 57, 1 [8]			10	4	20%
This work	**70**	**2**			**75%**

Table S2. Atomic composition of g-C_3N_4 and BP/g-C_3N_4 photocatalysts.

Sample	C atom %	N atom %	O atom %	P atom%

g-C_3N_4	46.71	49.68	3.61	0
BP/g-C_3N_4	46.70	47.41	3.59	3.30

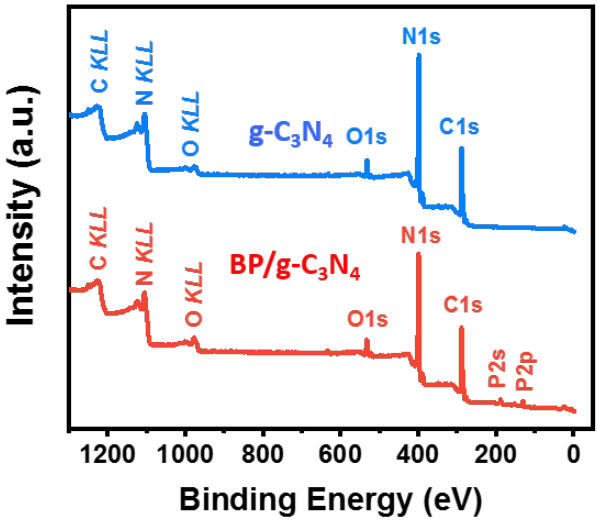

Figure S3. XPS survey spectra of g-C_3N_4 and BP/g-C_3N_4 nanosheets.

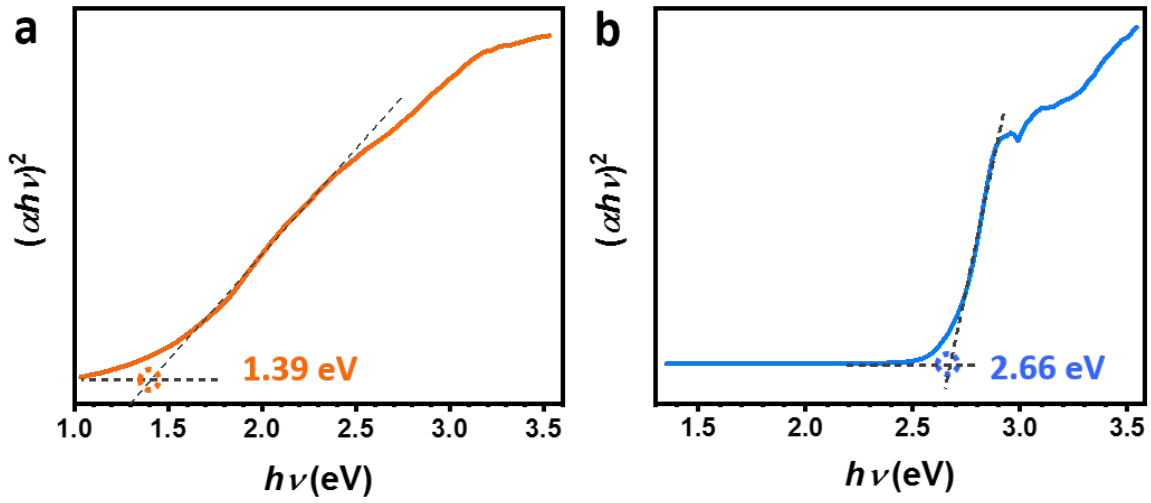

Figure S4. Representative direct Tauc plots of (a) BP nanosheets and (b) g-C_3N_4 samples used to determine their bandgap energy.

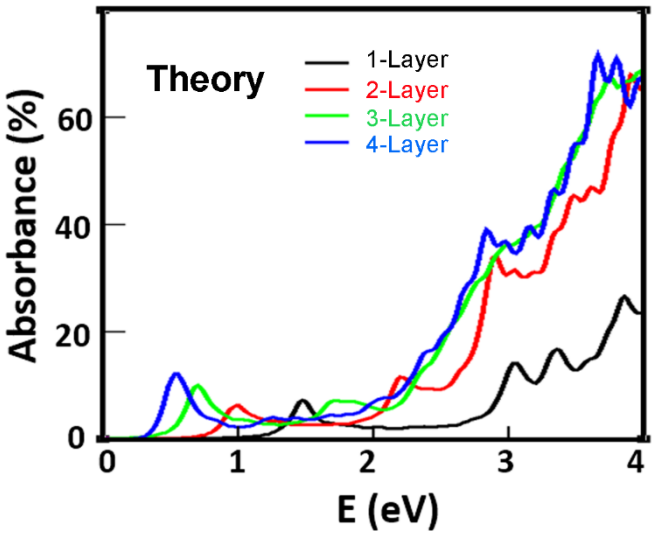

Figure S5. Theoretical calculations of the absorption spectra of BP with different numbers of layers (1-4 layers).

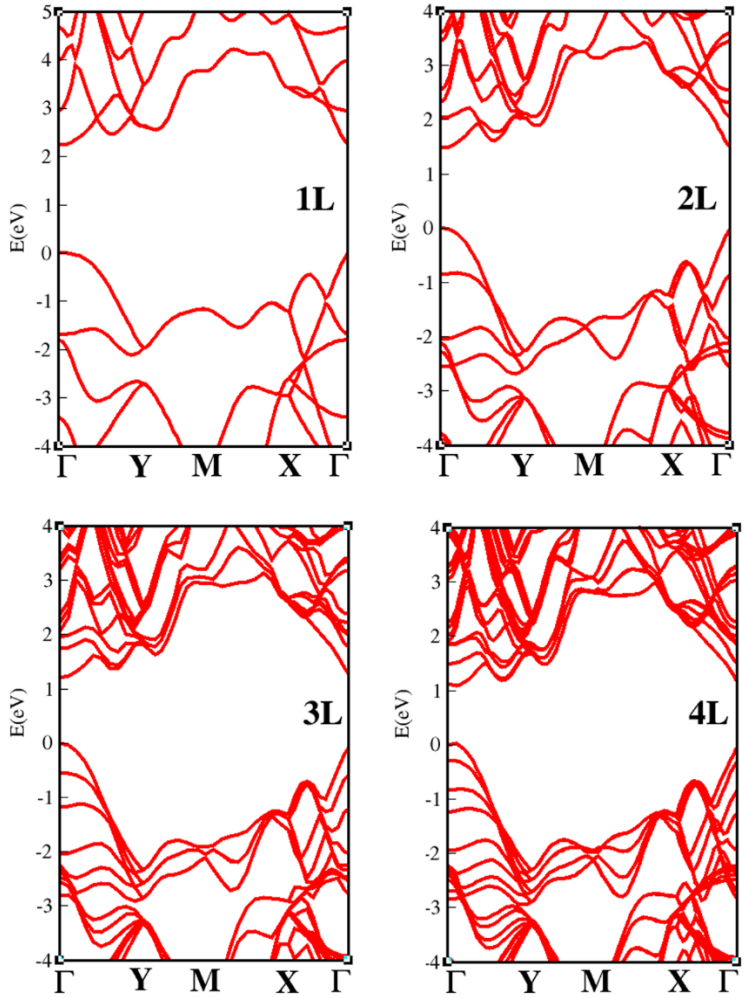

Figure S6. Calculated electronic GW band structures of BP with different numbers of layers (1-4 layers).

Table S3. Photocatalytic H_2 production rate under visible light ($\lambda > 420$ nm) irradiation.

References	Metal	Catalysts	H_2 evolution rate ($\mu mol\ g^{-1}\ h^{-1}$)
Nat. Mater. 2009, *8*, 76 [9]	3 wt% Pt	C_3N_4	106.94
Chem. Mater. 2015, 27, 4930 [10]	1 wt% Pt	H_2 treated g-C_3N_4	29.63
J. Catal. 2016, 342, 55 [11]	1 wt% Pt	g-C_3N_4 anatase/brookite TiO_2	29.97
Appl. Catal., B 2016, 192, 116 [12]	3 wt% Pt	Br-modified g-C_3N_4	960
Adv. Mater. 2017, 29, 1700008 [13]	3 wt% Pt	crystalline CN nanosheets	***1060***
Appl. Catal., B 2018, 224, 1 [14]	3 wt% Pt	O-doped C_3N_4 nanorods	732
Science 2015, *347*, 970 [15]	free	CDots-C_3N_4	105
Angew. Chem. Int. Ed. 2018, 57, 2160 [16]	free	BP/$BiVO_4$	160
This work	free	**BP/g-C_3N_4**	**384.17**

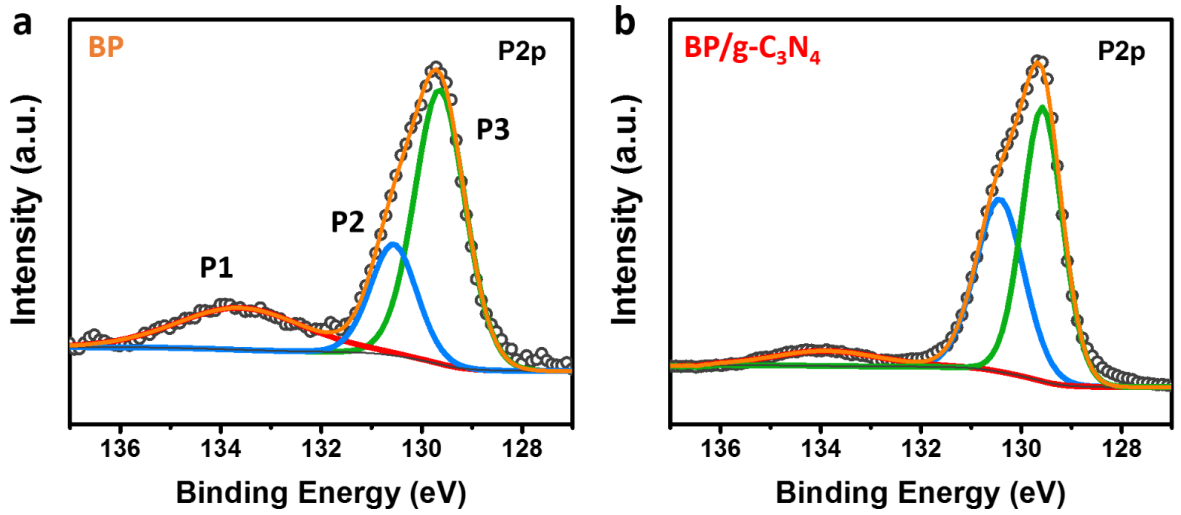

Figure S7. P2p XPS spectra of BP and BP/g-C_3N_4 samples after water splitting under visible light ($\lambda > 420$ nm) irradiation for 24 h.

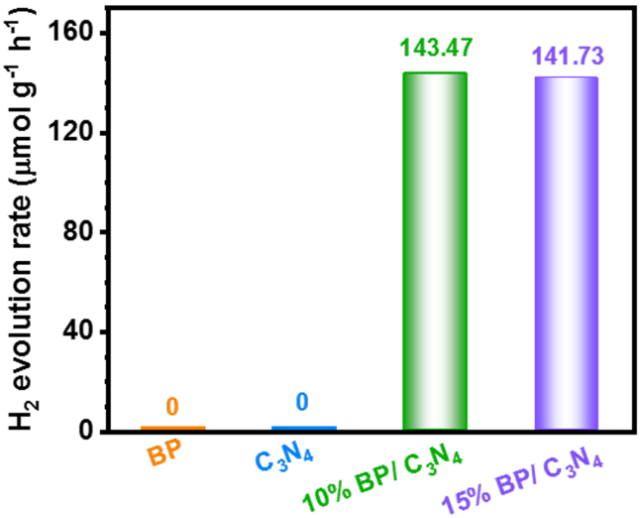

Figure S8. H_2 evolution rate achieved in the presence of BP (orange), g-C_3N_4 (blue), 10% BP/g-C_3N_4 (green) and 15% BP/g-C_3N_4 (purple) photocatalysts under $\lambda > 475$ nm light irradiation.

Table S4. The atomic percentage of P1, P2, and P3 in BP and BP/g-C_3N_4 photocatalysts estimated from Figure S3.

Sample	P1 %	P2 %	P3 %
BP	**21.6**	21.2	57.2
BP/g-C_3N_4	**7.5**	39.9	52.6

References

[1] a) Q. Zhang, J. Deng, Z. Xu, M. Chaker, D. Ma, *ACS Catal.* **2017**, *7*, 6225; b) Z. Xu, M. G. Kibria, B. AlOtaibi, P. N. Duchesne, L. V. Besteiro, Y. Gao, Q. Zhang, Z. Mi, P. Zhang, A. O. Govorov, L. Mai, M. Chaker, D. Ma, *Appl. Catal., B* **2018**, *221*, 77.

[2] P. Giannozzi, S. Baroni, N. Bonini, M. Calandra, R. Car, C. Cavazzoni, D. Ceresoli, G. L. Chiarotti, M. Cococcioni, I. Dabo, A. Dal Corso, S. de Gironcoli, S. Fabris, G. Fratesi, R. Gebauer, U. Gerstmann, C. Gougoussis, A. Kokalj, M. Lazzeri, L. Martin-Samos, N. Marzari, F. Mauri, R. Mazzarello, S. Paolini, A. Pasquarello, L. Paulatto, C. Sbraccia, S. Scandolo, G. Sclauzero, A. P. Seitsonen, A. Smogunov, P. Umari, R. M. Wentzcovitch, *J. Phys.-Condens. Matter* **2009**, *21*, 395502.

[3] A. Marini, C. Hogan, M. Gruning, D. Varsano, *Comput. Phys. Commun.* **2009**, *180*, 1392.

[4] A. H. Woomer, T. W. Farnsworth, J. Hu, R. A. Wells, C. L. Donley, S. C. Warren, *ACS Nano* **2015**, *9*, 8869.

[5] L. Chen, G. M. Zhou, Z. B. Liu, X. M. Ma, J. Chen, Z. Y. Zhang, X. L. Ma, F. Li, H. M. Cheng, W. C. Ren, *Adv. Mater.* **2016**, *28*, 510.

[6] W. Y. Lei, T. T. Zhang, P. Liu, J. A. Rodriguez, G. Liu, M. H. Liu, *ACS Catal.* **2016**, *6*, 8009.

[7] M. Zhu, S. Kim, L. Mao, M. Fujitsuka, J. Zhang, X. Wang, T. Majima, *J. Am. Chem. Soc.* **2017**, *139*, 13234.

[8] S. Yang, K. Zhang, A. G. Ricciardulli, P. Zhang, Z. Liao, M. R. Lohe, E. Zschech, P. W. M. Blom, W. Pisula, K. Mullen, X. Feng, *Angew. Chem., Int. Ed.* **2018**, *57*, 1.

[9] X. Wang, K. Maeda, A. Thomas, K. Takanabe, G. Xin, J. M. Carlsson, K. Domen, M. Antonietti, *Nat. Mater.* **2009**, *8*, 76.

[10] Q. Tay, P. Kanhere, C. F. Ng, S. Chen, S. Chakraborty, A. C. H. Huan, T. C. Sum, R. Ahuja, Z. Chen, *Chem. Mater.* **2015**, *27*, 4930.

[11] Q. L. Tay, X. H. Wang, X. Zhao, J. D. Hong, Q. Zhang, R. Xu, Z. Chen, *J. Catal.* **2016**, *342*, 55.

[12] Z.-A. Lan, G. Zhang, X. Wang, *Appl. Catal., B* **2016**, *192*, 116.

[13] H. Ou, L. Lin, Y. Zheng, P. Yang, Y. Fang, X. Wang, *Adv. Mater.* **2017**, *29*, 1700008.

[14] Y. Zeng, X. Liu, C. Liu, L. Wang, Y. Xia, S. Zhang, S. Luo, Y. Pei, *Appl. Catal., B* **2018**, *224*, 1.

[15] J. Liu, Y. Liu, N. Y. Liu, Y. Z. Han, X. Zhang, H. Huang, Y. Lifshitz, S. T. Lee, J. Zhong, Z. H. Kang, *Science* **2015**, *347*, 970.

[16] M. S. Zhu, Z. C. Sun, M. Fujitsuka, T. Majima, *Angew. Chem., Int. Ed.* **2018**, *57*, 2160.